Inorganic Chemistry Research

Article

Azo- and Hydrazo-Dipyridines in Halidometallate Structures

Simon Krakor (neé Schmitz), Leo Payen, Christopher Wallerius, Axel Klein*

University of Cologne, Faculty for Mathematics and Natural Sciences, Department of Chemistry, Institute for Inorganic Chemistry, Greinstraße 6, D-50939 Köln, Germany

Received: February 5, 2024; Accepted: February 28, 2024

Cite This: *Inorg. Chem. Res.* **2023**, *7*, 65-75. DOI: 10.22036/j10.22036.2024.441737.1159

Abstract: From reaction mixtures containing 1,2-di(pyridin-Y-yl)diazene derivatives ("azopyridines"; Y,Y'-azpy; Y = 2, 3, or 4) and metal precursors such as Cu(II), Co(II), Mn(II), Bi(III), and Fe(III) salts or elemental Sn, in aqueous concentrated HX (X = Cl, Br, I) solutions, we obtained single crystals of the new 1-D pseudo-perovskite structures (4,4'-azpyH$_2$)[Cu$_2$Cl$_6$], (4,4'-azpyH$_2$)[MnCl$_2$(H$_2$O)$_2$]Cl$_2$, (4,4'-azpyH$_2$)$_2$$^1{}_\infty$[Cu$_2I_4$(I$_3$)$_2$](I$_2$) (2,2'-hydpyH$_2$)$^1{}_\infty$[Cu$_2I_4$], (4,4'-hydpyH$_2$)$^1{}_\infty$[Cu$_2I_4$], and the 0-D pseudo-perovskite structure (4,4'-hydpyH$_2$)[BiI$_6$](I$_3$), along with non-perovskite salt-like structures. Some structures contain protonated azopyridinium (azpyH$_2^{2+}$) dications, obtained through protonation of the starting azopyridines, while others contain hydrazopyridinium (hydpyH$_2^{2+}$) cations, produced in a reduction-protonation reaction. Starting from Cu(II) salts, we found the metal reduced to Cu(I) in the presence of iodide, but not for chloride. The azopyridine-containing structures are easily discriminated from hydrazopyridine derivatives by their negligible C–N–N–C torsion angles and unequivocal *anti*-conformations. The hydrazopyridine moieties showed C–N–N–C torsions ranging from 99 to 133° and the conformations around the hydrazo –HN–NH– moiety are best described as *anti-clinal*.

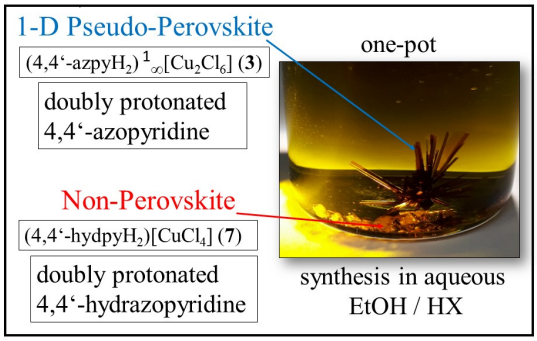

Keywords: Azodipyridines, Hydrazodipyridines, Organic-inorganic pseudo perovskites, Halidometalates

1. INTRODUCTION

In the last two decades the so called organic-inorganic hybrid perovskites with the formulae AM(II)X$_3$ or AM(III)X$_4$, where A$^+$ classically represents a small organic cation, frequently organic ammonium cations, where M(II) is a divalent group 14 cation, M(III) a trivalent group 15 cation, and X$^-$ are halides or pseudo-halides, have gained enormous interest due to their photo-semiconductor properties allowing the construction of photovoltaic cells with very high efficiencies.[1-7] The prototypical (MeNH$_3$)PbI$_3$ (usually abbreviated as MAPbI$_3$) forms the largest body of research and has been the subject of many in-depth studies seeking to understand the electronic properties of this material and close derivatives such as (MeNH$_3$)PbX$_{3-x}$Y$_x$ with X, Y = I, Br, or Cl[1-6] and eventually drive the development towards commercialisation.[8,9] More extended structural variations have come into focus mainly for four reasons. *i)* Toxicity and availability concerns on the large-scale use of lead-containing materials;[6,10-12] *ii)* Stability issues of (MeNH$_3$)PbI$_3$ and related derivatives;[1-3,5,6,11-15] *iii)* Desired variation of the electronic properties;[1-6,11,12,16-20] *iv)* The fabrication of lower dimensional (2-D and 1-D) materials.[1-3,6,12,16,17,20-31] An obvious approach to obtain 1-D or 2-D structures is the use of large, frequently aromatic organic cations.[1-4,6,12,17,20-32] Their aromatic cores can also enhance greatly the absorption of the materials through their π–π* transitions.[22-32]

The use of divalent and trivalent transition metals, as well as the trivalent main group metal Bi(III), for the construction of lead-free organic-inorganic perovskites is motivated by all four reasons. And in order to obtain lower dimensional perovskites, bifunctional (hetero)aromatic organic nitrogen bases (N-bases) were frequently used, to serve, in their protonated form, as bulky and in many cases also optically absorbing cations, following an established concept.[3,4,6,12,23-28,30-32]

In this contribution, we describe a very simple one-pot synthesis approach for organic-inorganic hybrid perovskites using chlorides or nitrates of Mn(II), Co(II), Cu(II), Bi(III), and Fe(III) or elemental Sn as metal precursors and the three isomeric 1,2-di(pyridin-Y-yl)diazenes ("azopyridines"; Y,Y'-azpy, Scheme 1) in aqueous HX (X = Cl, Br, I) to form the corresponding protonated dications azpyH$_2^{2+}$ as organic A^{2+} cations. The azopyridines were introduced as light-absorbing units.[33,34] Using this method, we obtained five 1-D

pseudo-perovskites and one so-called 0-D pseudo-perovskite structure, all containing protonated azopyridinium ($azpyH_2^{2+}$) dications, but also the hydrogenated hydrazopyridinium ($hydpyH_2^{2+}$) dications (Scheme 1). Further products of these reactions turned out to be halidometalates and halido salt of these cations, which we will only list in tables but not discuss.

A special focus in this study lies on Cu(II) as a typical transition metal ion having specific preferences for coordination geometries, such as square planar or tetragonally elongated (or compressed) octahedral.[18,19,35] However, the perovskite structure $ACuX_3$ is challenged by further stable complex species such as tetrahalidometalates $[CuX_4]^{2-}$ but also by coordination of the non-protonated N-bases to the metals, potentially leading to a plethora of different complexes or coordination polymers, containing halido and N-base ligands.[6,12,17,18,20,22,24,25,28] Furthermore, the formation of polyiodide containing structures from partial oxidation of I^- through redox-active metals such as Cu(II) or air might further thwart the formation of perovskite structures.

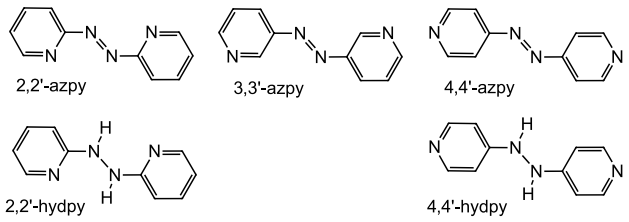

Scheme 1. Azopyridines (azpy) and hydrazopyridines (hydpy) reported in this study

2. RESULTS AND DISCUSSION

Preparation and analyses

The new materials were obtained through dissolving the metal salts $MnCl_2{\bullet}4H_2O$, $CoCl_2{\bullet}6H_2O$, $FeCl_3{\cdot}6H_2O$, $Co(NO_3)_2{\bullet}6H_2O$, $Cu(NO_3)_2{\bullet}3H_2O$, $Bi(NO_3)_3{\bullet}5H_2O$. or elemental tin in concentrate HX solution (X = Cl, Br, or I) and adding the azpy molecules in a 1:1 molar ratio (Table 1). The orange to red coloured products were obtained through as single crystals from the red (HI and HBr) to green (HCl) transparent reaction mixtures as described in detail in the Materials and Syntheses section in the Supplementary Materials (SM).

Through this procedure, we obtained various structures which can be divided into 0-D and 1-D pseudo-perovskites (marked in grey in Table 1 and marked with a blue frame in Scheme 2) and non-perovskite structures (red frame in Scheme 2).

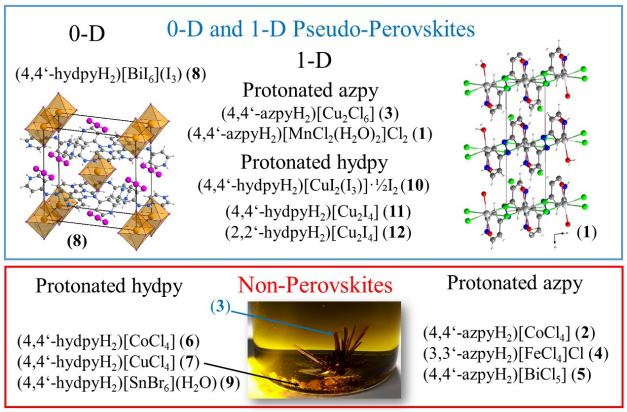

Scheme 2. Categorisation of the obtained compounds and structures. The arrows in the photograph indicate that compounds **3** and **7** stem from the same batch. Shown are also the structures of **1** and **8** for illustration

Some of the structures contain the double protonated azopyridinium $(Y,Y'\text{-}azpyH_2)^{2+}$ cations (compounds **1**, **2**, **3**, **4**, and **5**) while others contain the corresponding hydrazo derivatives $(Y,Y'\text{-}hydpyH_2)^{2+}$ (**6**, **7**, **8**, **9**, **10**, **11**, and **12**). The hydrazo-moieties in these compounds have obviously been generated *in situ* by a hydrogenation process, which we will discuss later. Both azopyridines and hydrazopyridines are protonated at the pyridine functions. Remarkably, compounds **3** (1-D pseudo-perovskite) and **7** (non-perovskite) were obtained from the same reaction batch (photograph in Scheme 2, bottom).

Unfortunately, concerning the oxidation states of the metals during the reactions and the observed *in situ* hydrogenation (reduction+protonation) of the azpy starting materials to the hydrazo derivatives, we have only

Table 1. Summary of synthetic approach and the obtained structures[a]

Metal ion	Organic molecule	HX	Compound	Space group	AMX-type	Dimension[b]	No.	CCDC
Mn^{2+}	4,4'-azpy	HCl	$(4,4'\text{-}azpyH_2)^1{}_\infty[MnCl_2(H_2O)_2]Cl_2$	$P2_1/c$	$AMX_2X'_2$	1-D	**1**	2062400
Co^{2+}	4,4'-azpy	HCl	$(4,4'\text{-}azpyH_2)[CoCl_4]$	$P2_1/n$	AMX_4	-	**2**	1951254
Cu^{2+}	4,4'-azpy	HCl	$(4,4'\text{-}azpyH_2)^1{}_\infty[Cu_2Cl_6]$	P-1	AM_2X_6	1-D	**3**	1951255
Fe^{3+}	3,3'-azpy	HCl	$(3,3'\text{-}azpyH_2)[FeCl_4]Cl$	$P2_1/m$	AMX_4X'	-	**4**	1951252
Bi^{3+}	4,4'-azpy	HCl	$(4,4'\text{-}azpyH_2)[BiCl_5]$	$C2/c$	AMX_5	-	**5**	1951253
Co^{2+}	4,4'-hydpy	HCl	$(4,4'\text{-}hydpyH_2)[CoCl_4]$	$P2_1/n$	AMX_4	-	**6**	1951258
Cu^2	4,4'-azpy	HCl	$(4,4'\text{-}hydpyH_2)[CuCl_4]$	$P4_1$	AMX_4	-	**7**	1951259
Bi^{3+}	4,4'-azpy	HI	$(4,4'\text{-}hydpyH_2)[BiI_6](I_3)$	$I2/m$	AMX_6X'	0-D	**8**	1951260
Sn^{4+}	4,4'-azpy	HBr	$(4,4'\text{-}hydpyH_2)[SnBr_6]{\cdot}H_2O$	$C2/c$	AMX_6	-	**9**	2062403
Cu^{2+}	4,4'-azpy	HI	$(4,4'\text{-}hydpyH_2)^1{}_\infty[CuI_2(I_3)](I_2)$	P-1	AMX_2X'	1-D	**10**	1951257
Cu^{2+}	4,4'-azpy	HI	$(4,4'\text{-}hydpyH_2)^1{}_\infty[Cu_2I_4]$	$Fdd2$	AM_2X_4	1-D	**11**	1951256
Cu^{2+}	2,2'-azpy	HI	$(2,2'\text{-}hydpyH_2)^1{}_\infty[Cu_2I_4]$	$P2_12_12_1$	AM_2X_4	1-D	**12**	1951251

[a]For details, see Experimental Section in the Supplementary Materials. Y,Y'-azpy = 1,2-di(pyridin-Y-yl)diazenes, Y,Y'-hydpy = 1,2-(pyridine-Y-yl)hydrazines. [b]Dimensions of the pseudo-perovskite structures are marked in grey.

limited information as, for all syntheses, we collected only the crystalline fractions and did not study the bulk material, washing solutions or mother liquors. For the same reasons, we can also not provide yields for the reactions. The purpose of this study was to get an overview over the possible structures resulting from such a simple synthesis approach.

Some of the crystalline materials were further characterised through Fourier-Transform (FT)-IR spectroscopy and thermogravimetric (TG)-differential thermal analysis (DTA) (see Supplementary Materials). From paramagnetic compounds containing Cu(II), Electron Paramagnetic Resonance (EPR) spectra were recorded.

In the following, we present in detail the five structures containing Cu and azopyridinium (Y,Y'-azpyH$_2$)$^{2+}$ dications (Figures 1 and 2) or hydrazopyridinium (Y,Y'-hydpyH$_2$)$^{2+}$ dications (Figure 3 to Figure 6). Further figures of these compounds and figures for all other structures can be found in the Supporting Materials (Figures S1 to S31)

Cu-containing structures

From reaction mixtures containing Cu(NO$_3$)$_2$·3H$_2$O and 4,4'-azopyridine in half-concentrated hydrochloric acid/EtOH solution, we obtained red-brown needles of the 1-D pseudo-perovskite (4,4'-azpyH$_2$)$^1{}_\infty$[Cu$_2$Cl$_6$] (**3**). Figure 1 shows the content of the unit cell (left) and

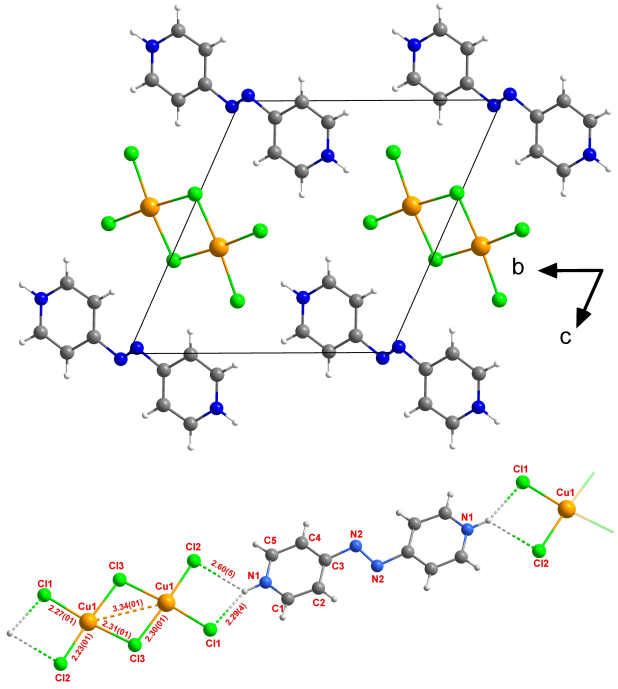

Figure 1. The unit cell of the 1-D pseudo-perovskite (4,4'-azpyH$_2$)$^1{}_\infty$[Cu$_2$Cl$_6$] (**3**) viewed along the crystallographic *a* axis (top), azpy-linkage between the [Cu$_2$Cl$_6$]$^{2-}$ units through hydrogen bonding in **3** (bottom).

N–H···Cl hydrogen bonds of moderate strength (right). The hydrogen bonding is very similar to what has been reported for a number of pyridinium tetrachlorido cuprates.[36-38] The (4,4'-azpyH$_2$)$^{2+}$ dications show an *anti*-conformation for the azo-pyridine moieties. The $^1{}_\infty$[Cu$_2$Cl$_6$]$^{2-}$ dianions represent a coordination network with a 4+2 elongated octahedral Cu coordination. Written in *Niggli* formalism, this is a $^1{}_\infty$[Cu$_2$Cl$^t{}_{1/1}$Cl$^k{}_{2/1}$Cl$^k{}_{3/1}$]$^{2-}$ network (Figure 2). The tetragonal elongation of the two axial Cl$^-$ ligands (Cu–Cl$_{vert}$) accounts to 36% of the equatorial Cu–Cl (Cu–Cl$_{horiz}$) bond lengths.

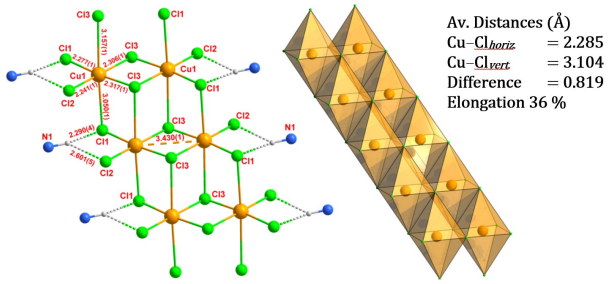

Figure 2. Two views on the $^1{}_\infty$[Cu$_2$Cl$_6$]$^{2-}$ coordination network of (4,4'-azpyH$_2$)$^1{}_\infty$[Cu$_2$Cl$_6$] (**3**).

A very similar $^1{}_\infty$[Cu$_2$Cl$_6$]$^{2-}$ motive was previously reported for (4,4'-bpyH$_2$)[Cu$_2$Cl$_6$] (4,4'-bpy = 4,4'-bipyridine)[37,38] and was also found in (melaH$_2$)[Cu$_2$Cl$_6$] (mela = 2,4,6-triamino-1,3,5-triazine.[39] They stand in contrast to isolated [Cu$_2$Cl$_6$]$^{2-}$ dianions as found in (Ph$_4$As)[CuCl$_3$][40] or (NPr$_4$)$_2$[Cu$_2$Cl$_6$],[41,42] or chains of such [Cu$_2$Cl$_6$]$^{2-}$ dimers with pentacoordinate Cu(II) as observed in (4-benzylpiperidinium)$_2$[Cu$_2$Cl$_6$][43] or (piperazinium)$_2$[Cu$_2$Cl$_6$] and further related structures which are known as so-called two-dimensional spin-gap magnets.[44] The X-band EPR of solid **3** showed a very broad signal centred at g = 2.0711, indicative for a Cu-centred radical species and huge line-broadening contributions of the Cl$^-$ anions, with their huge quadrupolar moment (I = 3/2) preventing the observation of Cu hyperfine splitting (I = 3/2 for $^{35/37}$Cu). While materials containing structurally isolated but magnetically connected [Cu$_2$Cl$_6$]$^{2-}$ units have been previously studied in detail,[44,45] compounds with a structural motive as in **3** have not been studied by EPR spectroscopy so far and we thus have, no comparison. The TG/DTA of **3** confirmed the composition of this compound, leaving CuCl$_2$ as residual and showing an exothermal signal at around 280° C for the decomposition of the azo-function (loss of N$_2$) (Figure S33).

Remarkably, from the same reaction batch from which we obtained (4,4'-azpyH$_2$)$^1{}_\infty$[Cu$_2$Cl$_6$] (**3**), we also found yellow octahedral specimen of the salt-like non-perovskite compound (4,4'-hydpyH$_2$)[CuCl$_4$] (**7**) containing reduced/hydrogenated 4,4'-hydpyH^{2+} dications (Figure 3). The hydrazo-pyridine core in these dications

shows a C–NH–NH–C torsion angle of 107.8(3)° (Table 2). Thus, the conformation around the N–N bond is best described as *anti-clinal*. TG/DTA confirmed the composition of **7**, with $CuCl_2$ as residual above 800° C. As for compound **3**, an exothermal signal for the N_2 loss at around 270° C was observed for **7** (Figure S34). The X-band EPR of solid **7** showed a broad signal centred at g = 2.1468 (Figure S35), in line with Cu-centred radical species and line-broadening from the Cl^- anions. At half-field we observed a sharper signal which we assign to the forbidden $\Delta M_S = \pm 2$ transition. Such half-field signals are frequently found for dinuclear complex species with ferromagnetic coupling of the unpaired spins of two Cu(II) ions resulting in an S = 1 ground state.[46-50] However, in **7** there are no dinuclear units. This implies that the Cu(II) centres in **7** show anti-ferromagnetic through-space coupling within the $[Cl_2CuCl_2\cdots Cl_2CuCl_2]^{4-}$ units shown in Figure 3.[51] Angle-dependent X-band EPR of **7** (Figure S36) are in line with a D_2d-flattened tetrahedral environment of the Cu(II) centres as found in the crystal structure.[52]

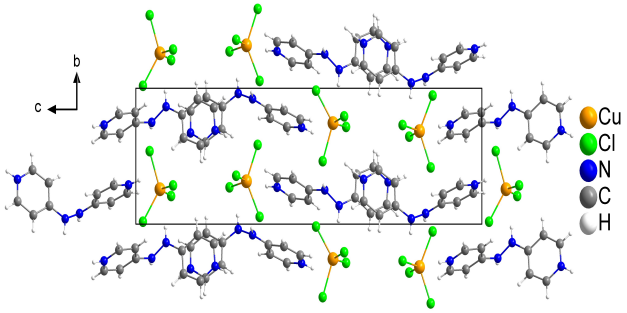

Figure 3. Salt-like non-perovskite structure of (4,4'-hydpyH$_2$)[CuCl$_4$] (**7**) viewed along the crystallographic *a*-axis.

Reacting $Cu(NO_3)_2{\bullet}3H_2O$ with 4,4'-azopyridine in half-concentrated hydroiodic acid in equimolar amounts afforded dark crystals with metallic appearance. Structure determination showed a 1-D pseudo-perovskite $[Cu_2I_4(I_3)_2]^{4-}$ unit in the structure of (4,4'-azpyH$_2$)$_2{}^1{}_\infty$[Cu$_2$I$_4$(I$_3$)$_2$]·1/2(I$_2$) (**10**) (Figure 4A and B).
From the viewpoint of the short I15-I15' distance of 2.7435(2) Å (Figure 4C), the 1-D network of **10** is best described as localised $[Cu_2I_4(I_3)_2]^{4-}$ dimers bridged by I_2 and not as to contain bridging I_8^{4-} units. From both descriptions it gets clear that the structure contains Cu(I), what was supported from X-band EPR spectroscopy which gave no signal. Thus, Cu(II) from the starting material has been reduced to Cu(I) under the reactions conditions. This is plausible from the very close potentials of the redox couples $I_2 + 2e^- \leftrightarrows 2\ I^-$ (E^0 = +0.621 V) [53] and Cu(II) + $1e^- \leftrightarrows$ Cu(I) (E^0 = +0.338 V) [53]. Interestingly, complexes of Cu(II) with azopyridines and iodide ligands have been previously reported such as the mononuclear [Cu(Y,Y'-azpy)X$_2$] (Y = 2, 3, 4; X = Cl, Br, I)[54] and the dinuclear complexes [Cu$_2$(2,2'-azpy)X$_2$] (X = Cl, Br, I),[55] but no coordination polymers containing Cu(II) and iodide.

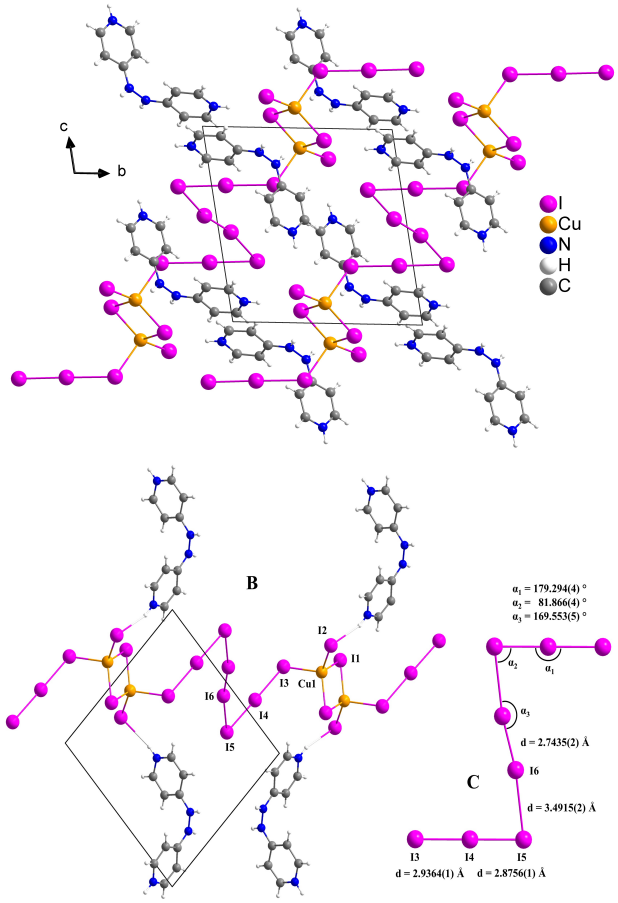

Figure 4. Crystal structure of (4,4'-azpyH$_2$)$_2{}^1{}_\infty$[Cu$_2$I$_4$(I$_3$)$_2$]·1/2(I$_2$) (**10**) viewed along the crystallographic *a*-axis (**A**). Linkage pattern of the 1-D pseudo-perovskite $[Cu_2I_4(I_3)_2]^{4-}$ dimer through an I_2 molecule in **10**) (**B**), with important angles and distances in the $(I_3)_2(I_2)^{4-}$ unit (**C**).

The same Cu(II) to Cu(I) reduction by iodide, has also happened during the synthesis of the two 1-D pseudo-perovskites **11** and **12**, which both contain Cu(I) (no EPR signals) in two different $^1{}_\infty[Cu_2I_4]^{2-}$ polymer strands (Figures 5 to 7).
The dianionic $^1{}_\infty[Cu_2I_4]^{2-}$ chains of (4,4'-hydpyH$_2$)$^1{}_\infty$[Cu$_2$I$_4$] (**11**) and (2,2'-hydpyH$_2$)$^1{}_\infty$[Cu$_2$I$_4$] (**12**) show different connection patterns, which becomes evident when looking at their *Niggli* nomenclature (Figure 7). While in **11** CuI_4 tetrahedra were 3/3 and 1/1 edge-sharing, for **12** they were 2,4 edge-sharing.
Similar $[Cu_2I_4]^{2-}$ coordination polymers as in **11** and **12** have been previously reported within the large family of literally hundreds of Cu(I)-I coordination polymers or oligomers.[56-59]

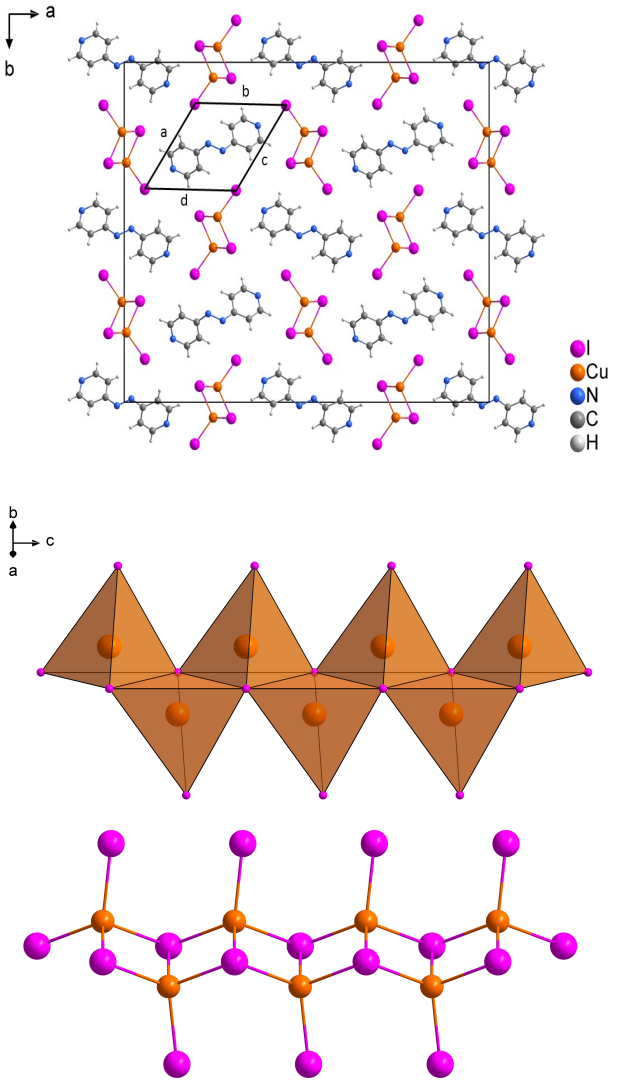

Figure 5. Crystal structure of the 1-D perovskite (4,4'-hydpyH$_2$)$^1{}_\infty$[Cu$_2$I$_4$] (**11**) viewed along the crystallographic *c* axis (left) and detail of the [Cu$_2$I$_4$]$^{2-}$-chains (right).

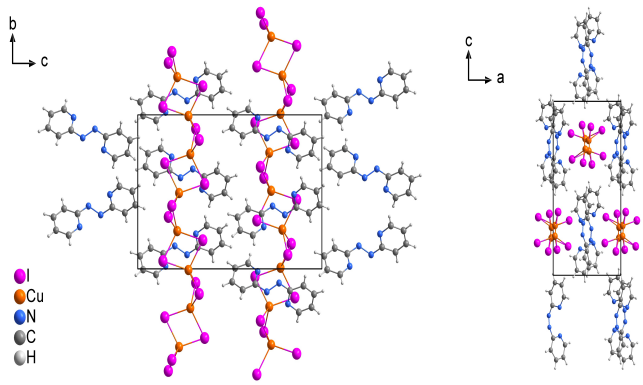

Figure 6. Views on the crystal structure of the 1-D pseudo-perovskite (2,2'-hydpyH$_2$)$^1{}_\infty$[Cu$_2$I$_4$] (**12**) along the crystallographic *a* and *b* axis.

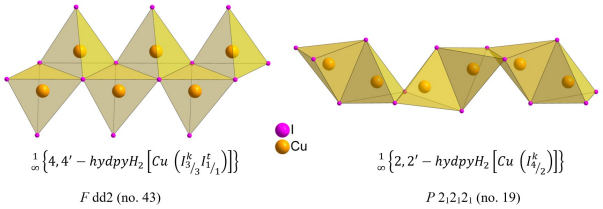

Figure 7. Connection pattern of the [Cu$_2$I$_4$]$^{2-}$-chains of (4,4'-hydpyH$_2$)$^1{}_\infty$[Cu$_2$I$_4$] (**11**) (left) and (2,2'-hydpyH$_2$)$^1{}_\infty$[Cu$_2$I$_4$] (**12**) (right), alongside with their formulas according to *Niggli* nomenclature.

Comparing azpy and hydpy structures

A crucial point in this study was the question if the obtained structures are azopyrines (azpy) or their corresponding hydrazopyridines (hydpy). The crucial structural parameters to distinguish between azpy and hydpy derivatives are the N–N bond length and the C–N–N–C torsion angle (Table 2). The azpyH$_2^{2+}$ dications moieties in the structures **1** to **5** showed N–N distances ranging from 1.04 to 1.25 Å, negligible C–N–N–C torsion angles and anti-conformations. The hydpyH$_2^{2+}$ dications had N–N distances ranging from 1.38 to 1.44 Å and completely variable C–N–N–C torsions from 99 to 133°.

Table 2. Essential structural parameters in the structures for the distinction between azo- (azpy) and hydrazo-dipyridines (hydpy)[a]

No.	Metal-containing compounds	N–N distance (Å)	C–N–N–C torsion (°)	Reaction medium	Figures
1	(4,4'-azpyH$_2$)[MnCl$_2$(H$_2$O)$_2$]Cl$_2$	1.216(4)	0.0(2)	HCl	S1–S3
2	(4,4'-azpyH$_2$)[CoCl$_4$]	1.184(5)	0.1(3)	HCl	S4–S5
3	(4,4'-azpyH$_2$)[Cu$_2$Cl$_6$]	1.248(3)	0.0(2)	HCl	1, 2, and S6–S8
4	(3,3'-azpyH$_2$)[FeCl$_4$]Cl	1.248(1)	0.00(7)	HCl	S9–S10
5	(4,4'-azpyH$_2$)[BiCl$_5$]	1.04(1)	2.4(7)	HCl	S11–S12
6	(4,4'-hydpyH$_2$)[CoCl$_4$]	1.380(3)	133.1(2)	HCl	S13–S14
7	(4,4'-hydpyH$_2$)[CuCl$_4$]	1.389(3)	107.8(3)	HCl	3 and S15–S16
8	(4,4'-hydpyH$_2$)[BiI$_6$](I$_3$)	1.43(1)	110(1)	HI	S17–S18
9	(4,4'-hydpyH$_2$)[SnBr$_6$]•(H$_2$O)	1.385(3)	101.4(3)	HBr	S19–S20
10	(4,4'-hydpyH$_2$)[CuI$_2$(I$_3$)]•1/2I$_2$	1.36(2)	99(1)	HI	4 and S21–S23
11	(4,4'-hydpyH$_2$)[Cu$_2$I$_4$]	1.37(1)	110(1)	HI	5 and S24–S25
12	(2,2'-hydpyH$_2$)[Cu$_2$I$_4$]	1.36(3)	129(3)	HI	6 and S26–S27
	Organic salts				
13	(4,4'-azpyH$_2$)Cl$_2$	1.233(2)	0.0(1)	HCl	S28–S29
14	(4,4'-hydpyH$_2$)I$_2$	1.388(5)	102.2(6)	HI	S30–S31

[a]From single crystal XRD (details in the Experimental Section).

The conformations around the hydrazo –HN–NH– moiety are best described as *anti-clinal*. This data allows unequivocal discrimination between azopyridines and hydrazo derivatives and include also a corresponding pair of salt-like compounds (4,4'-azpyH$_2$)Cl$_2$ (**13**) and (4,4'-hydpyH$_2$)I$_2$ (**14**).

In contrast to the literally hundreds of complexes and coordination polymers of azopyridines,[54,55,60-67] complexes and coordination polymers of hydrazopyridines are scarce [66–71]. This includes a small number of complexes such as the dinuclear [Ru$_2$(NH$_3$)$_{10}$(4,4'-hydpy)](PF$_6$)$_4$[63] and a number of Zn(II), Cd(II), Co(II), or Ni(II) containing metal-organic frameworks[68-71] were reported. The structural data reported therein is in perfect agreement with our findings.

Reduction/hydrogenation of the azopyridines

While the protonation of the pyridine function in the azpy and hydpy molecules is not unexpected, since the pyridine function represents the more basic N atoms, the reduction/hydrogenation of azpy to hydpy derivatives was a bit surprising. As reported earlier,[63,67,72-74] the azopyridine molecules (azpy) are prone to reduction to their hydrazine derivatives (hydpy).

We studied the electrochemistry of the 4,4'-azpy derivative and found two reversible reduction waves in the cyclic voltammograms at –1.26 and –1.76 V, vs. ferrocene/ferrocenium, in dry THF solution (Figure S37). In the presence of acetic acid, an irreversible reduction wave at –1.07 V was observed, which has an anodic counterpart at –0.27 V. The –1.07 V calculate to about –0.25 V vs. normal hydrogen electrode (NHE) in the same solvent, which means that the two-electron reduction (azpy/azpy^{2-}), combined with the protonation of azpy^{2-} to hydpy, is generally facile.

In our synthesis approach for perovskite structures, we found that when using 2,2'- and 4,4'-azpy together with an excess of HI, the species found in the solid structure is always the corresponding hydpy molecule or the hydpyH$_2^{2+}$ dication. We assumed, that under the reaction conditions the redox pair I$^-$/I$_2$ (E^0 in water = +0.621 V vs. NHE[53]) is able to reduce/hydrogenate azpy. The presence of a metal cation seems not to be necessary as the synthesis of (4,4'-hydpyH$_2$)I$_2$ (**14**) from 4,4'-azpy in HI shows (structure in Figures S30 and S31).

When running the reactions in conc. HCl we did not expect the reduction of azpy to hydpy derivatives due to the much higher redox potential of the Cl$^-$/Cl$_2$ redox pair (E^0 in water = +1.396 vs. NHE[53]). And indeed, many structures containing azpyH$_2^{2+}$ dications were obtained from HCl solutions. However, we also obtained the compounds (4,4'-hydpyH$_2$)[CuCl$_4$] (**7**) and (4,4'-hydpyH$_2$)[CoCl$_4$] (**6**) as exceptions. Despite of having a far larger reduction potential than I$^-$, it seems that Cl$^-$ can still donate electrons to azpy in the systems Cu(II)/azpy/Cl$^-$ or Co(II)/azpy/Cl$^-$. An alternative explanation is the protonation of metal-bound azpy and subsequent oxidation of the metal as has been reported for Ru(II)/4,4'azpy complexes.[63] As we did not follow the bulk reaction, but collected only crystalline products out of the reaction batch, we can only speculate on this reaction so far. In future work, we will study this in more detail.

3. MATERIALS AND METHODS

Instrumentation. UV-vis Absorption spectra were recorded with Varian Cary 05E or Cary 50 scan spectrophotometers. **Elemental Analyses** were obtained using a HEKAtech CHNS EuroEA 3000 analyzer. **FT-IR Spectra** were measured in ATR mode using a Perkin Elmer 400 FT-IR spectrometer. **Electrochemical** measurements were carried out in 0.1 M *n*-Bu$_4$NPF$_6$/THF solution using a three-electrode configuration (glassy carbon working electrode, Pt counter electrode, Ag/AgCl reference electrode) and a Metrohm Autolab PGSTAT30 potentiostat and function generator. The ferrocene/ferrocenium couple served as internal reference.

XRD Single Crystal Structure Analysis. Crystals were obtained from concentrated reaction mixtures through evaporation in the fume hood (details in the Syntheses Section in the Supplementary Materials). X-ray diffraction measurements were performed at 293(2) K using an IPDS II (STOE and Cie.) or a Gemini CCD S Ultra diffractometer (Oxford Diffraction) both operating with Mo-Kα radiation (λ = 0.71073 Å) and employing ω-φ-2θ scan technique. The structures were solved with the programs *WinGX*[75] and *Olex2* (v. 1.2).[76] Direct methods were applied using SIR-2014[77] and refinement was carried out with SHELXT-2015,[78] employing full-matrix least-squares methods on $F_0^2 < 2\sigma(F_0^2)$. Numerical absorption corrections (X-RED32 V1.31; Stoe & Cie, 2005)[79] were performed after optimizing the crystal shapes using X-SHAPE V1.06 (Stoe & Cie, 1999).[79] Absorption corrections of the "Multi-scan"-type were performed using *SADABS* (Bruker).[80] The non-hydrogen atoms were refined with anisotropic displacement parameters without any constraints. The hydrogen atoms were included by using appropriate riding models. The final structure visualisation was carried out using *Diamond* (v. 3.2k and 4.6.3).[81] Full data (CCDC numbers in Table 1) can be obtained free of charge at https://summary.ccdc.cam.ac.uk/structures or from the Cambridge Crystallographic Data Centre, 12 Union Road, Cambridge, CB2 1EZ UK (fax: +44-1223 336033 or E-mail: deposit@ccdc.cam.ac.uk).

Materials and Syntheses. Materials and Syntheses are described in the Supplementary Materials.

4. CONCLUSIONS

Using the simple synthesis approach of mixing azopyridines (Y,Y'-azpy; Y = 2, 3, or 4) and metal precursors (salts of Cu(II), Co(II), Mn(II), Bi(III), or Fe(III) or elemental Sn) dissolved in concentrated aqueous HX (X = Cl, Br, I), we obtained the new 1-D pseudo-perovskite structures (4,4'-azpyH$_2$)$^1{}_\infty$[Cu$_2$Cl$_6$], (4,4'-azpyH$_2$)$^1{}_\infty$[MnCl$_2$(H$_2$O)$_2$]Cl$_2$, (4,4'-azpyH$_2$)$_2{}^1{}_\infty$[Cu$_2$I$_4$(I$_3$)$_2$]·1/2(I$_2$), (2,2'-hydpyH$_2$)$^1{}_\infty$[Cu$_2$I$_4$], (4,4'-hydpyH$_2$)$^1{}_\infty$[Cu$_2$I$_4$], and the 0-D pseudo-perovskite structure (4,4'-hydpyH$_2$)[BiI$_6$](I$_3$). However, many more structures we obtained from such procedures were non-perovskite halidometalates such as (4,4'-hydpyH$_2$)[CuCl$_4$]. This clearly demonstrates that obtaining the desired 1-D or 2-D perovskite structures using such simple synthesis approaches is challenged by the formation of other possible structures. At least, from the aqueous HX conditions we could rule out the formation of complexes with the (hydr)azopyridines. The observed hydrogenations/reductions of the azopyridines (azpy) to the corresponding hydrazines (hydpy) were resulting from yet not completely understood redox processes, which will be studied in further detail in the future. We will also attempt in future work, to reproduce the interesting Cu-containing 1-D perovskite structures mentioned above. The most interesting finding is that Cu(II) seems to be very suitable in replacing Pb(II) in the field of low-dimensional organic-inorganic hybrid perovskites. However, we also found that Cu(II) clearly rules out the use of iodide.

Supplementary Materials. The following supporting information can be downloaded at: https://www.xxx, Details on **Materials and Syntheses**. Table S1: List of starting materials and commercial suppliers. Table S2: Summary of synthetic approach and the obtained structures. Figure S1: ORTEP plot of (4,4'-azpyH$_2$)[MnCl$_2$(H$_2$O)$_2$]Cl$_2$ (**1**) at 50% probability. Figure S2: Crystal structure of (4,4'-azpyH$_2$)[MnCl$_2$(H$_2$O)$_2$]Cl$_2$ (**1**) viewed along the crystal. *a*-axis. Figure S3: Crystal structure of (4,4'-azpyH$_2$)[MnCl$_2$(H$_2$O)$_2$]Cl$_2$ (**1**) viewed along the crystallographic *b*-axis. Figure S4: ORTEP plot of (4,4'-azpyH$_2$)[CoCl$_4$] (**2**) at 50% probability. Figure S5: Crystal structure of (4,4'-azpyH$_2$)[CoCl$_4$] (**2**) viewed along the crystallographic *a*-axis. Figure S6: ORTEP plot of (4,4'-azpyH$_2$)[Cu$_2$Cl$_6$] (**3**). Figure S7: Crystal structure of (4,4'-azpyH$_2$)[Cu$_2$Cl$_6$] (**3**) viewed along the crystallographic *a*-axis. Figure S8: Linkage through hydrogen bonding in the 1D pseudo-perovskite (4,4'-azpyH$_2$)[Cu$_2$Cl$_6$] (**3**). Figure S9: ORTEP plot of (3,3'-azpyH$_2$)[FeCl$_4$]Cl (**4**) at 50% probability. Figure S10: Crystal structure of (3,3'-azpyH$_2$)[FeCl$_4$]Cl (**4**) viewed along the crystallographic *a*-axis. Figure S11: ORTEP plot of (4,4'-azpyH$_2$)[BiCl$_5$] (**5**) at 50% probability. Figure S12: Crystal structure of (4,4'-azpyH$_2$)[BiCl$_5$] (**5**) viewed along the crystallographic *b*-axis. Figure S13: ORTEP plot of (4,4'-hydpyH$_2$)[CoCl$_4$] (**6**) at 50% probability. Figure S14: Crystal structure of (4,4'-hydpyH$_2$)[CoCl$_4$] (**6**) viewed along the crystallographic *a*-axis. Figure S15: ORTEP plot of (4,4'-hydpyH$_2$)[CuCl$_4$] (**7**) at 50% probability. Figure S16: Crystal structure of (4,4'-hydpyH$_2$)[CuCl$_4$] (**7**) viewed along the crystallographic *a*-axis. Figure S17: ORTEP plot of (4,4'-hydpyH$_2$)[BiI$_6$](I$_3$) (**8**) at 50% probability. Figure S18: Structure of (4,4'-hydpyH$_2$)[BiI$_6$](I$_3$) (**8**) viewed along the crystallographic *a*-axis. Figure S19: ORTEP plot of (4,4'-hydpyH$_2$)[SnBr$_6$]·(H$_2$O) (**9**) at 50% probability. Figure S20: Crystal structure of (4,4'-hydpyH$_2$)[SnBr$_6$]·(H$_2$O) (**9**) viewed along the crystallographic *a*-axis. Figure S21: ORTEP plot of (4,4'-hydpyH)[CuI$_2$(I$_3$)]·1/2I$_2$ (**10**) at 50% probability. Figure S22: Crystal structure of (4,4'-hydpyH$_2$)[CuI$_2$(I$_3$)]·1/2I$_2$ (**10**) viewed along the crystallographic *a*-axis. Figure S23: Linkage pattern of the [Cu$_2$I$_4$(I$_3$)$_2$]$^{4-}$ dimer through an I$_2$ molecule in (4,4'-azpyH$_2$)$_2{}^1{}_\infty$[Cu$_2$I$_4$(I$_3$)$_2$]·1/2(I$_2$) (**10**) with important angles and distances in the (I$_3$)$_2$(I$_2$)$^{4-}$ unit. Figure S24: ORTEP plot of (4,4'-hydpyH$_2$)[Cu$_2$I$_4$] (**11**) at 50% probability. Figure S25: Crystal structure of (4,4'-hydpyH$_2$)[Cu$_2$I$_4$] (**11**) viewed along the crystallographic *a*-axis. Figure S26: ORTEP plot of (2,2'-hydpyH$_2$)[Cu$_2$I$_4$] (**12**) at 50% probability. Figure S27: Crystal structure of (2,2'-hydpyH$_2$)[Cu$_2$I$_4$] (**12**) viewed along the crystallographic *a*-axis. Figure S28: ORTEP plot of (4,4'-azpyH$_2$)Cl$_2$ (**13**) at 50% probability. Figure S29: Crystal structure of (4,4'-azpyH$_2$)Cl$_2$ (**13**) viewed along the crystallographic *a*-axis. Figure S30: ORTEP plot of (4,4'-hydpyH$_2$)I$_2$ (**14**) at 50% probability. Figure S31: Crystal structure of (4,4'-hydpyH$_2$)I$_2$ (**14**) viewed along the crystallographic *c*-axis. Figure S32: FT-IR spectrum of (4,4'-azpyH$_2$)[Cu$_2$Cl$_6$] (**3**). Figure S33: TG/DTA of (4,4'-azpyH$_2$)[Cu$_2$Cl$_6$] (**3**). Figure S34: TG/DTA of (4,4'-hydpyH$_2$)[CuCl$_4$] (**7**). Figure S35: X-band EPR-spectra of (4,4'-azpyH$_2$)[Cu$_2$Cl$_6$] (**3**) in the solid at 298 K. Figure S36: X-band EPR-spectra of (4,4'-hydpyH$_2$)[CuCl$_4$] (**7**). Figure S37: Cyclic voltammograms of 4,4'-azpy.

CONFLICTS OF INTEREST

The authors declare no conflict of interest.

ACKNOWLEDGMENTS

We thank the group for crystal structure analyses of the department, Dr. Jörg Neudörfl, Dr. Ingo Pantenburg and Silke Kremer.

AUTHOR INFORMATION

Corresponding Author

Axel Klein: Email: axel.klein@uni-koeln.de. *ORCID*: 0000-0003-0093-9619

Author(s)

Simon Krakor (neé Schmitz), Leo Payen, Christopher Wallerius

REFERENCES

1. O. Almora, D. Baran, G. C. Bazan, C. I. Cabrera, S. Erten-Ela, K. Forberich, F. Guo, J. Hauch et al.. Device Performance of Emerging Photovoltaic Materials (Version 3). *Adv. Energy Mater.* **2023**, *13*, 2203313 (128).
2. O. Almora, D. Baran, G. C. Bazan, C. Berger, C. I. Cabrera, K. R. Catchpole, S. Erten-Ela et al.. Device Performance of Emerging Photovoltaic Materials (Version 2). *Adv. Energy Mater.* **2021**, *11*, 2102526 (1-41).
3. A. Soultati, M. Tountas, K. K. Armadorou, A. R. b. M. Yusoff, M. Vasilopoulou, M. K. Nazeeruddin, Synthetic approaches for perovskite thin films and single-crystals. *Energy Adv.* **2023**, *2*, 1075-1115.
4. J. Euvrard, Y. Yan, D. B. Mitzi, Electrical doping in halide perovskites. *Nat. Rev. Mater.* **2021** *6*, 531-549.
5. X. Guo, C. Burda, Coordination engineering toward high performance organic-inorganic hybridperovskites, *Coord. Chem. Rev.* **2016**, *320-321*, 53-65.
6. B. Saparov, D. B. Mitzi, Organic-Inorganic Perovskites: Structural Versatility for Functional Materials Design. *Chem. Rev.* **2016**, *116*, 4558-4596.
7. C. Huang, E. Gajewiak, A. Wright, W. Rodriguez-Kazeem, D. Heift, J. C. Bear, A comparative meta-analysis of gains in efficiency in Pb and Sn-based perovskite solar cells over the last decade. *Z. Anorg. Allg. Chem.* **2023**, *649*, e202300045 (1-13).
8. L. Jonathan, L. J. Diguna, O. Samy, M. Muqoyyanah, S. A. Bakar, M. D. Birowosuto, A. El Moutaouakil, Hybrid Organic-Inorganic Perovskite Halide Materials for Photovoltaics towards Their Commercialization. *Polymers* **2022**, *14*, 1059.
9. T. D. Siegler, A. Dawson, P. Lobaccaro, D. Ung, M. E. Beck, G. Nilsen, L. L. Tinker, The Path to Perovskite Commercialization: A Perspective from the United States Solar Energy Technologies Office. *ACS Energy Lett.* **2022**, *7*, 1728-1734.
10. EU phasing out use of Pb: https://echa.europa.eu/hot-topics/lead, last accessed on 27.02.2024.
11. K. Sakhatskyi, R. A. John, A. Guerrero, S. Tsarev, S. Sabisch, T. Das, G. J. Matt, S. Yakunin, I. Cherniukh, M. Kotyrba, Yu. Berezovska, M. I. Bodnarchuk, S. Chakraborty, J. Bisquert, M. V. Kovalenko, Assessing the Drawbacks and Benefits of Ion Migration in Lead Halide Perovskites. *ACS Energy Lett.* **2022**, *7*, 3401-3414.
12. C. Coccia, M. Moroni, L. Malavasi, Chiral Metal Halide Perovskites: Focus on Lead-Free Materials and Structure-Property Correlations. *Molecules* **2023**, *28*, 6166.
13. J. Zhuang, J. Wang, F. Yan, Review on Chemical Stability of Lead Halide Perovskite Solar Cells. *Nano-Micro Lett.* **2023**, *15*, 84.
14. T. A. Chowdhury, Md. A. B. Zafar, Md. S. -Ul. Islam, M. Shahinuzzaman, M. A. Islam, M. U. Khandaker, Stability of perovskite solar cells: issues and prospects. *RSC Adv.* **2023**, *13*, 1787-1810.
15. G. Annohene, G. Tepper, Moisture Stability of Perovskite Solar Cells Processed in Supercritical Carbon Dioxide. *Molecules* **2021**, *26*, 7570.
16. A. M. Ganose, C. N. Savory, D. O. Scanlon, Beyond methylammonium lead iodide: prospects for the emergent field on ns^2 containing solar absorbers. *Chem. Commun.* **2017**, *53*, 20-44.
17. L. Mao, J. Chen, P. Vishnoi, A. K. Cheetham, The Renaissance of Functional Hybrid Transition-Metal Halides. *Acc. Mater. Res.* **2022**, *3*, 439-448.
18. L. Theofylaktos, K. O. Kosmatos, E. Giannakaki, H. Kourti, D. Deligiannis, M. Konstantakou, T. Stergiopoulos, Perovskites with d-block metals for solar energy applications. *Dalton Trans.* **2019**, *48*, 9516-9537.
19. W. Liu, Z. Zhou, H. Li, Y. Lv, H. Tong, J. Zhu, G. Ouyang, New Strategy for Optimizing the Properties of Copper Halide Organic-Inorganic Hybrid Lighting-emitting Materials. *Chem.-Eur. J.* **2022**, *28*, e202202478 (1-8).
20. M. Ptak, A. Sieradzki, M. Šimenas, M. Maczka, Molecular spectroscopy of hybrid organic-inorganic perovskites and related compounds. *Coord. Chem. Rev.* **2021**, *448*, 214180.
21. R. L. Z. Hoye, J. Hidalgo, R. A. Jagt, J. -P. Correa-Baena, T. Fix, J. L. MacManus-Driscoll, The Role of Dimensionality on the Optoelectronic Properties of Oxide and Halide Perovskites, and their Halide Derivatives. *Adv. Energy Mater.* **2022**, *12*, 2100499 (1-59).
22. X. Li, J. M. Hoffman, M. G. Kanatzidis, The 2D Halide Perovskite Rulebook: How the Spacer Influences Everything from the Structure to Optoelectronic Device Efficiency. *Chem. Rev.* **2021**, *121*, 2230-2291.
23. W. T. M. Van Gompel, R. Herckens, K. Van Hecke, B. Ruttens, J. D'Haen, L. Lutsen, D. Vanderzande, Low-Dimensional Hybrid Perovskites Containing an Organic Cation with an Extended Conjugated System: Tuning the Excitonic Absorption Features. *ChemNanoMat.* **2019**, *5*, 323-327.

24. N. I. Selivanov, Yu. A. Rozhkova, R. Kevorkyants, A. V. Emeline, D. W. Bahnemann, The effect of organic cations on the electronic, optical and luminescence properties of 1D piperidinium, pyridinium, and 3-hydroxypyridinium lead trihalides. *Dalton Trans.* **2020**, *49*, 4390-4403.
25. P. Walter, E. Kaifer, H. Herrmann, H. Wadepohl, O. Hübner, H. -J. Himmel, Redox-Active Guanidines with One or Two Guanidino Groups and Their Integration in Low-Dimensional Perovskite Structures. *Eur. J. Inorg. Chem.* **2019**, *2019*, 4147-4160.
26. Y. -Q. Hu, H. -Y. Hui, W. -Q. Lin, H. -Q. Wen, D. -S. Yang, G. -D. Feng, Crystal and Band-Gap Engineering of One-Dimensional Antimony/Bismuth-Based Organic-Inorganic Hybrids. *Inorg. Chem.* **2019**, *58*, 16346-16353.
27. G. García-Espejo, D. Rodríguez-Padrón, M. Pérez-Morales, R. Luque, G. de Miguel, L. Camacho, Mechanochemical synthesis of one-dimensional (1D) hybrid perovskites incorporating polycyclic aromatic spacers: highly fluorescent cation-based materials. *J. Mater. Chem. C*, **2018**, *6*, 7677-7682.
28. J. V. Passarelli, D. J. Fairfield, N. A. Sather, M. P. Hendricks, H. Sai, C. L. Stern, S. I. Stupp, Enhanced Out-of-Plane Conductivity and Photovoltaic Performance in n = 1 Layered Perovskites through Organic Cation Design. *J. Am. Chem. Soc.* **2018**, *140*, 7313-7323.
29. Y. Wei, P. Audebert, L. Galmiche, J. -S. Lauret, E. Deleporte, Photostability of 2D Organic-Inorganic Hybrid Perovskites. *Materials* **2014**, *7*, 4789-4802.
30. S. Zhang, P. Audebert, Y. Wei, A. A. Choueiry, G. Lanty, A. Bréhier, L. Galmiche, G. Clavier, C. Boissière, J. -S. Laurent, E. Deleporte, Preparation and Characterization of Luminescent Two Dimensional Organic-inorganic Perovskite Semiconductors. *Materials* **2010**, *3*, 3385-3406.
31. M. -G. Ju, J. Dai, L. Ma, Y. Zhou, X. C. Zeng, Zero-Dimensional Organic-Inorganic Perovskite Variant: Transition between Molecular and Solid Crystal. *J. Am. Chem. Soc.* **2018**, *140*, 10456-10463.
32. A. Latini, S. Quaranta, F. Menchini, N. Lisi, D. Di Girolamo, O. Tarquini, M. Colapietro, L. Barba, N. Demitri, A. Cassetta, A novel water-resistant and thermally stable black lead halide perovskite, phenyl viologen lead iodide $C_{22}H_{18}N_2(PbI_3)_2$. *Dalton Trans.* **2020**, *49*, 2616-2627.
33. H. Ren, P. Yang, H. Yu, Recent Progress in Azopyridine-Containing Supramolecular Assembly: From Photoresponsive Liquid Crystals to Light-Driven Devices. *Molecules* **2022**, *27*, 3977.
34. H. Ren, P. Yang, F. M. Winnik, Azopyridine: a smart photo- and chemo-responsive substituent for polymers and supramolecular assemblies. *Polym. Chem.* **2020**, *11*, 5955-5961.
35. M. A. Halcrow, Jahn-Teller distortions in transition metal compounds, and their importance in functional molecular and inorganic materials. *Chem. Soc. Rev.* **2013**, *42*, 1784-1795.
36. D. K. Kumar, A. Ballabh, D. A. Jose, P. Dastidar, A. Das, How Robust Is the N−H···Cl2−Cu Synthon? Crystal Structures of Some Perchlorocuprates. *Cryst. Growth Des.* **2005**, *5*, 651-660.
37. C. Näther, I. Jeß, M. Bolte, 4,4'-Bipyridylium di-μ-chlorotetrachlorodicuprate(II): a redetermination. *Acta Crystallogr., Sect E: Structure Rep.* **2001**, *57*, m78-m79.
38. R. D. Willett, R. E. Butcher, C. P. Landee, B. Twamley, Two halide exchange in copper(II) halide dimers: (4,4'-bipyridinium)$Cu_2Cl_{6-x}Br_x$. *Polyhedron* **2006**, *25*, 2093-2100.
39. R. Mesbeh, B. Hamdi, R. Zouari, Elaboration, structural, spectroscopy, DSC investigations and Hirshfeld surface analysis of a one-dimensional self-assembled organic-inorganic hybrid compound. *J. Mol. Struct.* **2017**, *1128*, 205-214.
40. C. Chow, R. D. Willett, B. C. Gerstein, Magnetic Susceptibility of One-Dimensional Linear Chains of Ferromagnetically Coupled $Cu_2X_6^{2-}$ Dimers. *Inorg. Chem.* **1975**, *14*, 205-207.
41. G. Hu, E. M. Holt, Bis(tetrapropylammonium) Hexachlorodicuprate(II). *Acta Crystallogr., Sect. C: Cryst. Struct. Commun.* **1994**, *50*, 1212-1214.
42. A. Oueslati, A. Bulou, F. Calvayrac, K. Adil, M. Gargouri, F. Hlel, Infrared, polarized Raman and ab initio calculations of the vibrational spectra of $[N(C_3H_7)_4]_2Cu_2Cl_6$ crystals. *Vib. Spectrosc.* **2013**, *64*, 10-20.
43. S. O'Brien, R. M. Gaura, C. P. Landee, B. L. Ramakhrishna, R. D. Willett, Magneto-structural Correlations in Chains of Bifolded $Cu_2Cl_6^{2-}$ Dimers. *Inorg. Chim. Acta* **1988**, *141*, 83-89.
44. V. N. Glazkov, T. S. Yankova, J. Sichelschmidt, D. Hüvonen, A. Zheludev, Electron spin resonance study of anisotropic interactions in a two-dimensional spin-gap magnet $(C_4H_{12}N_2)(Cu_2Cl_6)$. *Phys. Rev. B* **2012**, *85*, 054415.
45. S. V. Voitekhovich, A. S. Lyakhov, L. S. Ivashkevich, F. Schleife, R. Schnorr, B. Kersting, P. N. Gaponik, Synthesis and characterization of 5-amino-1,3-di-*tert*-butyl-2*H*-tetrazol-1-ium bis[di-l-chlorido-bis [dichloridocuprate(II)]]. *Inorg. Chim. Acta* **2014**, *419*, 124-129.
46. A. Klein, K. Butsch, S. Elmas, C. Biewer, D. Heift, S. Nitsche, I. Schlipf, H. Bertagnolli, Oxido-pincer complexes of copper(II)-an EXAFS and EPR study of mono- and binuclear $[(pydotH_2)CuCl_2]_n$ (n = 1 or 2). *Polyhedron* **2012**, *31*, 649-656.
47. J. T. Brewster II, H. D. Root, H. Zafar, G. D. Thiabaud, A. C. Sedgwick, J. He, V. M. Lynch, J. L.

Sessler,. Synthesis and Characterization of a Binuclear Copper(II)-dipyriamethyrin Complex: [Cu_2(dipyriamethyrin)(μ^2-1,1-acetato)$_2$]. *Molecules* **2020**, *25*, 1446.
48. S. K. Hoffmann, D. Towle, W. E. Hatfield, P. Chaudhuri, K. Wieghardt, *Inorg. Chem.* **1985**, *24*, 1307-1312.
49. K. Butsch, A. Sandleben, M. H. Dokoohaki, A. R. Zolghadr, A. Klein,. Pyridine-2,6-dicarboxylic acid esters (pydicR_2) as O,N,O-pincer ligands in Cu^{II} complexes. *Inorganics* **2019**, *7*, 53 (1-19).
50. G. H. Clever, S. J. Reitmeier, T. Carell, O. Schiemann, Antiferromagnetic Coupling of Stacked Cu^{II}–Salen Complexes in DNA. *Angew. Chem., Int. Ed.* **2010**, *49*, 4927-4929.
51. M. -H. Whangbo, H. -J. Koo, R. K. Kremer, Spin Exchanges between Transition Metal Ions Governed by the Ligand p-Orbitals in Their Magnetic Orbitals. *Molecules* **2021**, *26*, 531.
52. A. Winter, K. Thiel, A. Zabel, T. Klamroth, A. Pöppl, A. Kelling, U. Schilde, A. Taubert, P. Strauch, Tetrahalidocuprates(II)-structure and EPR spectroscopy. Part 2: tetrachloridocuprates(II). *New J. Chem.* **2014**, *38*, 1019-1030.
53. A. J. Bard, R. Parsons, J. Jordan, "Standard potentials in aqueous solutions", Marcel Dekker Inc. New York and Basel **1985**; ISBN: 0-8247-7291-1.
54. R. Grzeskowiak, C. Whatley, M. Goldstein, Metal complexes of azopyridines-IV [l]. Infrared and Raman spectral studies of zinc complexes of 2,2'-, 3,3'- and 4,4'-azopyridines, and copper complexes of 2,2'-azopyridine. *Spectrochim. Acta A* **1975**, *31*, 1577-1594.
55. D. A. Baldwin, A. B. P. Lever, R. V. Parish, Complexes of 2,2'-Azopyridine with Iron(II), Cobalt(II), Nickel(II), Copper(I), and Copper(II). An Infrared Study. *Inorg. Chem.* **1969**, *8*, 107-115.
56. J. Conesa-Egea, F. Zamora, P. Amo-Ochoa, Perspectives of the smart Cu-Iodine coordination polymers: A portage to the world of new nanomaterials and composites. *Coord. Chem. Rev.* **2019**, *381*, 65-78,
57. Z. -H. Jiang, P. Shang, Z. -W. Jiang, T. Lu, H. -M. Guan, Y. -H. Li, L. -C. Gui, X. -F. Jiang, Self-Assembly of an Anionic $[Cu_5I_8]^{3-}$ Supramolecular Cluster Driven by Ion-Pair Interaction and Catalytic Properties. *Inorg. Chem.* **2023**, *62*, 15403-15411.
58. C. Ren, J. Li, X. Zhang, Y. Niu, Photocatalytic Degradation of Ciprofloxacin with Supramolecular Materials Consisting of Nitrogenous Organic Cations and Metal Salts. Photocatalytic Degradation of Ciprofloxacin with Supramolecular Materials Consisting of Nitrogenous Organic Cations and Metal Salts. *Catalysts* **2023**, *13*, 1134.
59. K. Wang, A. K. Chinnam, N. Petrutik, E. P. Komarala, Q. Zhang, Q. -L. Yan, R. Dobrovetsky, M. Gozin, Iodocuprate-containing ionic liquids as promoters for green propulsion. *J. Mater. Chem. A* **2018**, *6*, 22819-22829.
60. S. Maity, S. Kundu, T. Weyhermüller, P. Ghosh, Tris(2,2′-azobispyridine) Complexes of Copper(II): X-ray Structures, Reactivities, and the Radical Nonradical Bis(ligand) Analogues. *Inorg. Chem.* **2015**, *54*, 1300-1313.
61. R. Grzeskowiak, C. Whatley, M. Goldstein, Metal complexes of azopyridines-IV [l]. Infrared and Raman spectral studies of zinc complexes of 2,2'-, 3,3'- and 4,4'-azopyridines, and copper complexes of 2,2'-azopyridine. *Spectrochim. Acta A* **1975**, *31*, 1577-1594.
62. D. A. Baldwin, A. B. P. Lever, R. V. Parish, Complexes of 2,2'-Azopyridine with Iron(II), Cobalt(II), Nickel(II), Copper(I), and Copper(II). An Infrared Study. *Inorg. Chem.* **1969**, *8*, 107-115.
63. J. -P. Launay, M. Tourrel-Pagis, J. -F. Lipskier, V. Marvaud, C. Joachim, Control of Intramolecular Electron Transfer by a Chemical Reaction. The 4,4'-Azopyridine/1,2-Bis(4-pyridyl)hydrazine System. *Inorg. Chem.* **1991**, *30*, 1033-1038.
64. W. Kaim, Complexes with 2,2'-azobispyridine and related 'S-frame' bridging ligands containing the azo function. *Coord. Chem. Rev.* **2001**, *219-221*, 463-488.
65. A. A. Swatiputra, D. Mukherjee, S. Dinda, S. Roy, K. Pramanik, S. Ganguly, Electron transfer catalysis mediated by 3d complexes of redox non-innocent ligands possessing an azo function: a perspective. *Dalton Trans.* **2023**, *52*, 15627-15646.
66. D. Gupta, A. K. Gaur, H. Kumar, S. Singh, S. Venkataramani, Light-Switchable Metal Complexes: Introducing Photoresponsive Behaviour Through Azoheteroarenes. *ChemPhotoChem*. **2023**, *7*, e202300068 (1-24).
67. S. Panda, S. Dhara, A. Singh, S. Dey, G. K. Lahiri, Metal-coordinated azoaromatics: Strategies for sequential azo-reduction, isomerization and application potential. *Coord. Chem. Rev.* **2023**, *475*, 214895.
68. X. -M. Liu, R. -B. Lin, J. -P. Zhang, X. -M. Chen, Low-Dimensional Porous Coordination Polymers Based on 1,2-Bis(4-pyridyl)hydrazine: From Structure Diversity to Ultrahigh CO_2/CH_4 Selectivity. *Inorg. Chem.* **2012**, *51*, 5686-5692.
69. X. Li, D. Sensharma, K. Koupepidou, X. -J. Kong, M. J. Zaworotko, The Effect of Pendent Groups upon Flexibility in Coordination Networks with Square Lattice Topology. *ACS Mater. Lett.* **2023**, *5*, 2567-2575.
70. M. A. W. Lawrence, S. C. Lorraine, K. -A. Wilson, K. Wilson, Review: Voltammetric properties and

applications of hydrazones and azo moieties. *Polyhedron* **2019**, *173*, 114111.
71. A. J. Bellamy, I. S. MacKirdy, C. E. Niven, Cyclic Voltammetry of Azopyridines, Phenylazopyridines, and Azobenzene in Acetonitrile and Dimethylformamide. *J. Chem. Soc., Perkin Trans. 2*, **1983**, *1983*, 183-185.
72. J. L. Sadler, A. J. Bard, The Electrochemical Reduction of Aromatic Azo Compounds. *J. Am. Chem. Soc.* **1968**, *90*, 1979-1989.
73. L. -J. Farrugia, WinGX and ORTEP for Windows: an update. *J. Appl. Cryst.* **2012**, *45*, 849-854.
74. O. V. Dolomanov, L. J. Bourhis, R. J. Gildea, J. A. K. Howard, H. Puschmann, OLEX2: a complete structure solution, refinement and analysis program. *J. Appl. Cryst.* **2009**, *42*, 339-341.
75. M. C. Burla, R. Caliandro B. Carrozzini, G. L. Cascarano, C. Cuocci, C. Giacovazzo, M. Mallamo, A. Mazzone, G. Polidori, Crystal structure determination and refinement via SIR2014. *J. Appl. Cryst.* **2015,** *48*, 306-309.
76. G. M. Sheldrick, Crystal Structure Refinement with SHELXL. *Acta Crystallogr. Sect. C Struct. Chem.* **2015**, *71*, 3-8.
77. Stoe & Cie. X-RED32 V1.31 (**2005**) and X-SHAPE V1.06 (**1999**) Software, Stoe & Cie GmbH, Darmstadt, Germany.
78. Bruker (**2001**). SADABS. Bruker AXS Inc., Madison, Wisconsin, USA.
79. K. Brandenburg, **1997-2020** Crystal Impact GbR, Bonn, Germany.